RESEARCH ARTICLE



A new particle for measuring mass transfer in turbulence

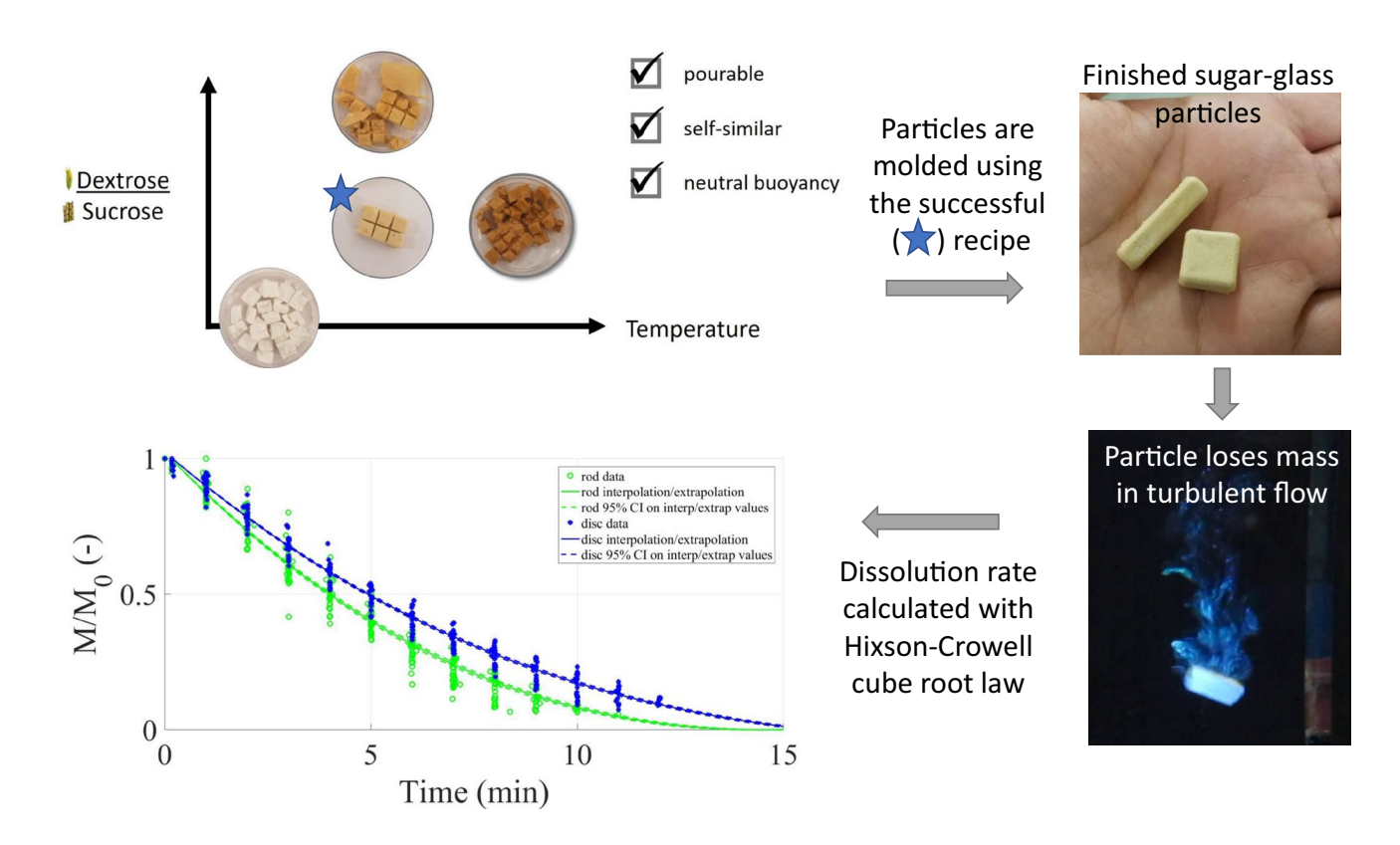
Theresa B. Oehmke¹ • Evan A. Variano¹

Received: 29 April 2020 / Revised: 10 October 2020 / Accepted: 19 October 2020 / Published online: 8 January 2021 © The Author(s) 2021

Abstract

We present a method for creating a new type of model particle that allows us to measure the mass transfer rate from the particle surface to the surrounding water. We use hollow glass spheres and sugar to create neutrally buoyant particles in a variety of molded shapes. These particles are an alternative to traditional gypsum objects for measuring mass transfer, with the important characteristic of being neutrally buoyant. This is an inexpensive method that allows for custom particle shapes to be manufactured with different densities. We test the utility of these particles by measuring their dissolution rates in homogeneous, isotropic turbulence in our laboratory turbulence tank. Our measurements fit our proposed model, and give a faster dissolution rate for rod-shaped particles than for disc-shaped ones.

Graphic abstract



[☐] Theresa B. Oehmke toehmke@berkeley.edu



Department of Civil and Environmental Engineering, University of California, Berkeley, CA, USA

16 Page 2 of 10 Experiments in Fluids (2021) 62:16

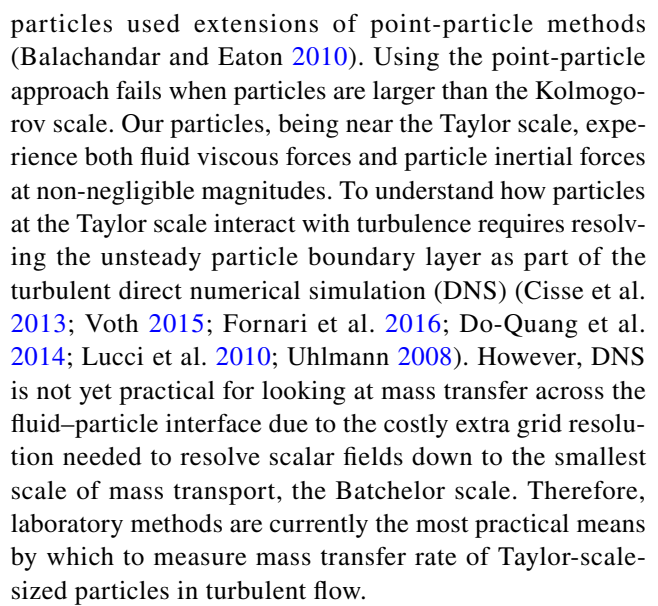
1 Introduction

Mass transfer is an important topic in many areas of science and engineering (Bird and Stewart 2007; Nazaroff and Alvarez-Cohen 2001). Industrial examples include chemical reactors (Boon-Long et al. 1978; Sano et al. 1974) and pharmaceuticals (Grijseels et al. 1981). Environmental examples include the moderation of biomass decay by bacteria (Nazaroff and Alvarez-Cohen 2001; Stocker et al. 2008; Kiørboe et al. 2002) and copepods (Lombard et al. 2013), zooplankton finding mates (Bagøien and Kiørboe 2005), and ctenophore locomotion (Sasson et al. 2018). Some of these particle sizes lie within the inertial subrange (Byron et al. 2015), the scale of turbulence which has a nearly constant rate of energy transfer from large scales to small scales without significant energy loss due to viscosity. For particles in this size range, we are interested in the relationship between their shape, motion, and flux.

Particles whose size are in the inertial subrange of turbulence are influenced by unsteady fluid forcing (from the turbulent flow), by the boundary layer surrounding the particle, and by inertia from the particle mass. This is an interesting regime in which particles are large enough to inertially cross fluid streamlines, yet small enough to be moved by turbulent fluctuations. In addition to size, we consider shape as an important feature because shape and size work together to determine how a particle reacts to ambient turbulent forcing (Bordoloi and Variano 2017). The influence of shape on rotation has recently become the subject of investigation (Voth and Soldati 2017; Pujara et al. 2018) and rotation likely influences mass transfer. Defining the shape-motion-flux relationship will help clarify fundamental questions about particle-turbulence interactions within the inertial subrange.

Particles smaller than the Kolmogorov scale, the smallest lengthscale of turbulence, move with a Stokesian response to a time-varying linear shear flow. Simulations of this motion in turbulence demonstrate differences in the ways rods and dics move in turbulent flows (Byron et al. 2015; Shima and Voth 2014; Chevillard and Meneveau 2013; Pujara et al. 2019). Rods tend to spin more around their symmetry axis while discs have a tendency to tumble (rotate around the axis perpendicular to the symmetry axis) (Byron et al. 2015). It is currently an open question whether the tendency of a certain shape towards tumbling versus spinning persists for particles in the inertial subrange. Such particles have lengthscales longer than the Kolmogorov scale, but smaller than the energy-containing scales that begin the turbulent 'cascade.' A scale in between those two extremes is the Taylor lengthscale (Pope 2000).

Previous work by Haugen et al. (2017) on mass transfer in turbulent suspensions of sub-Kolmogorov scale



Direct measurements of mass transfer rates traditionally used gypsum (plaster of Paris) to measure flow velocity via dissolution rates in both laboratory and field experiments (Porter et al. 2000; Angradi and Hood 1998; Baird and Atkinson 1997; Pachon-Rodriguez and Colombani 2013). Before going to the field, laboratory calibrations were used to correlate flowrate with dissolution (Angradi and Hood 1998; Baird and Atkinson 1997; Pachon-Rodriguez and Colombani 2013; Thompson and Glenn 1994). Plaster of Paris was molded into shapes such as spheres (Porter et al. 2000), cubes (Angradi and Hood 1998), and corals (Baird and Atkinson 1997), before being fixed in place as water flowed past. The results of these experiments were reliable only under certain conditions: the flow statistics of the calibration flow system needed to match the flow statistics of the natural environment where the method was deployed. More recent studies used X-ray computed tomography (CT) scanning and digital holographic microscopy, respectively, to calculate the dissolution rate of gypsum forms (Feng et al. 2017; Chang 2013). These methods did not require comparisons between the rate of dissolving in a laboratory flow and that of the field to find a dissolution rate, leading to more flexibility in experimental set-ups. Nonetheless, these objects were still fixed in space.

Studies by Huang et al. (2015) have taken a similar approach of using dissolution to characterize water motion coupled with shape dynamics. In these experiments, hard candies (instead of gypsum) were dissolved in laminar high-speed flows to study the evolution of particle shape and the receding candy surface. This process showed shape convergence of cylinders and hemispheres to a steady terminal form (Huang et al. 2015). The overall dissolution rate of the sugar increased with the square root of flow speed, and the volume of the submerged body vanished quadratically in time. Due to the shape-flow feedback, this experiment



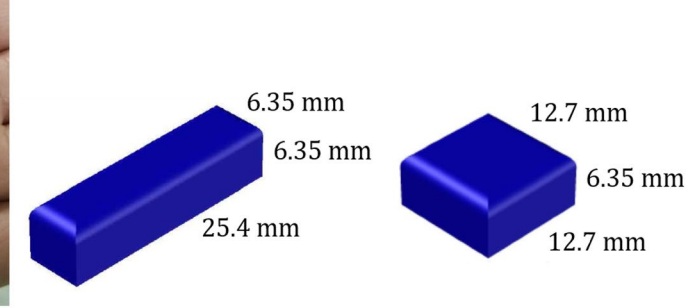
resulted in a moving boundary layer problem (Huang et al. 2015). Using scaling laws, Huang et al. (2015) were able to find a recession velocity based only on relevant scales such as diffusivity and boundary layer thickness. Their experiments show evolution of a solid body towards a state of uniform shear and therefore uniform material flux (Huang et al. 2015). While these experiments could hold insights into the behavior of our freely moving sugar particles, their experiments were performed in laminar flow and simplified to a 2D model. Turbulence, on the other hand, is inherently 3D and unsteady.

Some research teams have investigated freely moving particles in turbulence; however, these studies only looked at granular particles (Sano et al. 1974) and spheres (Sano et al. 1974; Machicoane et al. 2013; Levins and Glastonbury 1972; Boon-Long et al. 1978). In the experiments by Sano et al. (1974) and Levins and Glastonbury (1972), mass transfer rates of granular particles and spherical ion exchange beads of relatively small sizes (60-600 μ m in diameter) were characterized using the Schmidt (Sc = v/D) and Sherwood $(Sh = kd_n/D)$ numbers (Sano et al. 1974; Levins and Glastonbury 1972). The Schmidt number describes the ratio of momentum diffusion to mass diffusion with v being the kinematic viscosity $[(length)^2/(time)]$ and D the mass diffusivity $[(length)^2/(time)]$. The Sherwood number is often written as a function of the Schmidt number, and relates the convective mass transfer rate to the diffusion rate. In the Sherwood number, k is the mass transfer coefficient [(length)/(time)]and d_n is the particle diameter; D is the mass diffusivity, same as in the Schmidt number. Boon-Long et al. (1978) did similar experiments with spherical benzoic acid particles (2.2–4.3 mm in diameter) dissolving in water (Boon-Long et al. 1978). We are interested in doing freely moving particle experiments as well, but with larger particles in a variety of anisotropic shapes.

Machicoane et al. (2013) used larger particles (1–3 cm in diameter) to study the heat transfer rates of melting ice balls. The authors placed ice balls in a turbulent von Kármán apparatus with parallel lighting and used afocal shadowgraphy to measure melting rates of the spheres. In comparing ice balls that were fixed in space with those that

Fig. 1 Neutrally buoyant dissolving particles using our new manufacturing method. Rod-shaped particles are shown on the left and disc-shaped particles are shown on the right. The rod-shaped particles pictured are matched by volume to the disc-shaped particles





of the fixed ice sphere became ellipsoidal over its melting period due to the anisotropy of the flow, while the ice sphere that was freely moving melted isotropically in all of the tested flows (Machicoane et al. 2013). The authors predict this could be due to the particle's ability to rotate on itself while it is melting (Machicoane et al. 2013).

In this study, we focus on freely moving particles which

could freely move about, the authors found that the shape

In this study, we focus on freely moving particles which dissolve along their Lagrangian trajectories. To conduct experiments with particles suspended in a turbulent flow, the particles need to be neutrally buoyant. Neither gypsum, ice, nor sugar alone meet this requirement. Therefore we have developed a sugar-glass-sphere compound that can be used to measure dissolution in a similar manner as gypsum. In this paper, we explain the method for manufacturing such particles and use example particles to explore how shape affects the mass transfer rate from a particle's surface in a turbulent flow.

2 Methods

Two different shapes were tested in this experiment, shown in Fig. 1. The first shape, called 'discs,' had dimensions of 12.7 mm \times 12.7 mm \times 6.35 mm and the second shape, called 'rods,' had dimensions of 6.35 mm \times 6.35 mm \times 25.4 mm. These dimensions provided two different aspect ratios (aspect ratio = symmetry axis length : degenerate axis length) for examination while keeping volume constant. The disc-like particles had an aspect ratio of 1/2, and the rod-like particles had an aspect ratio of 4. Volume-matched particles were chosen because studies show that particle volume, and not surface area or aspect ratio, control the rotation of Taylor-scale-sized particles suspended in isotropic turbulence (Bordoloi and Variano 2017; Byron et al. 2015). Because rotation and mass transfer both depend on fluid shear near the particle surface, we take rotation as an initial prediction of mass transfer behavior.



16 Page 4 of 10 Experiments in Fluids (2021) 62:16

2.1 Fabrication of particles

The particles were made from a mixture of sucrose, dextrose, and hollow glass spheres, which was heated and poured into molds where they cooled and hardened. A series of positive and negative molds was created (shown in Fig. 2). The first mold is a positive mold of the particles, and was made using the Monoprice Mini 3D printer and PLA plastic. The second mold, made out of silicone, is a negative mold of the particles. Vegetable oil was used as a release agent and applied to the positive mold before the mixing of silicone began. The silicone was mixed by combining reagents A and B of PlatSil® 73–15 Liquid Rubber according to the manufacturer's direction, using equal proportions by weight. Mixed silicone was poured into the oiled positive mold and set for 5 h before it was demolded. Excess rubber around the edges was trimmed with a razor blade.

Once the silicone molds were created, they were filled with the cooked sugar-glass recipe to make the particles. The recipe required mixing 24.0 g of sucrose (Fisher Scientific S5-3), 1.5 g of dextrose (Fisher Scientific BP350-1), and 5.55 g of hollow glass spheres (3MTM Glass Bubbles K37) in a 100 mL beaker. Then 10 mL of deionized water was added to help combine the ingredients into a slurry. The ingredients were added one-by-one and the combined cumulative mass of the ingredients and the beaker was recorded between consecutive additions. The stirrer bar and thermometer were added to the beaker and recorded. Recording the mass of each component was essential to having a consistent water concentration in the final particle. The size of the beaker was important for achieving the proper consistency of the mixture before it was molded. The thermometer gave the most accurate temperature readings when it was submerged in at least one inch of the mixture. Working with this constraint, a 100 mL beaker provided the most consistent results regarding temperature measurements and volume capacity of the beaker to avoid the mixture over-boiling.

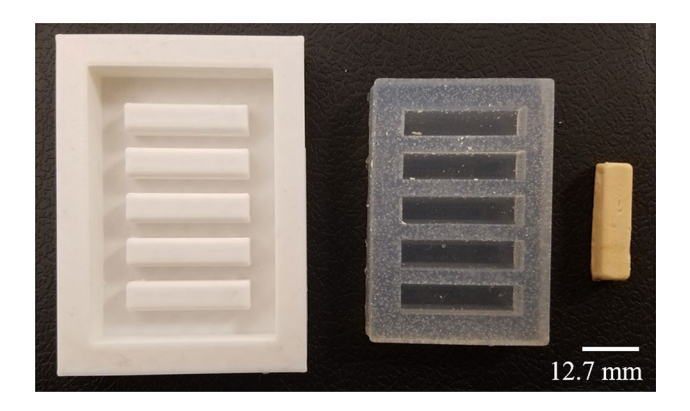


Fig. 2 3D printed positive rod-shaped mold, negative silicone mold, and finished neutrally buoyant rod-shaped particle



The mixture was heated on a hot plate with an average steady-state surface temperature of 256 °C \pm 2 °C. As the mixture cooked, the total mass was monitored to measure the amount of water that had evaporated. When the water concentration reached 5% of the mixture's mass, the mixture was poured into the silicone molds. A water concentration of 5% was normally achieved at a temperature of 121 °C \pm 2 °C (about 20 min after boiling, characterized by bubble formation, began). At this point, the mixture was light tan in color, and a filament of it would easily snap if dropped into a glass of cold water. One batch of the above recipe filled approximately two of the silicone molds pictured in Fig. 2.

The cooked slurry solidified quickly after it was removed from the heat, which made casting the particles a time-sensitive process. The beaker was insulated with a neoprene beverage sleeve to help mitigate this problem. The rapid cooling did not leave enough time for any air bubbles introduced when pouring the mixture to rise and escape from the mold before the shape hardened. To minimize the number of trapped bubbles, the mixture was poured into the center of the mold cavity; the mixture flowed out from the center to fill the corners. This technique slightly reduced the amount of large air pockets trapped along the edges and corners of a hardened particle. Those particles for which air was trapped inside during molding were discarded at a later stage. A glass stirrer bar was used to aid in pouring the mixture from the beaker to the mold. After the molds were filled, they were leveled by scraping the stirrer bar across the top of the mold. This leveling process occasionally created a vacuum resulting in a depression on the surface of the particles. Particles with severe depressions were not used for testing. After the mixture was poured into the molds, it was left to cool to room temperature before being demolded and sanded to remove any jagged edges.

Rod- and disc-shaped particles each had their individual molding challenges. The majority of the disc-like particles did not trap air pockets within them, but the mixture often did not flow all the way to the corners of the mold cavity, leaving the edges of the particles rounder than the intended shape. For the rod-like particles, the corners presented less of a problem. However, on average, there were more rodlike particles that contained hidden air pockets than disc-like particles. An example of this can be seen in Fig. 3, where the rod-like particle dissolved irregularly due to the hollow cavities. The cavity inside the particle did not become apparent until the particle started to dissolve. When cavities appeared, the particle and the data were discarded and the experiment was repeated with a new particle. Some batches of particles had more air pockets in them than others, depending on how quickly the mixture was poured into the molds after reaching the ideal water concentration. The results presented here include only particles that maintained their shape as they were tested.

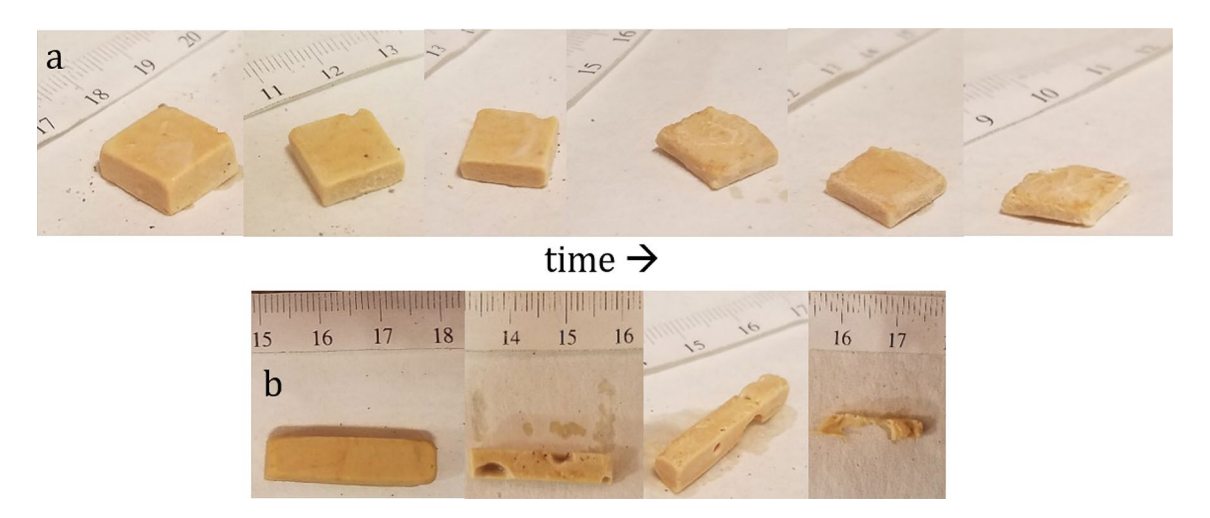


Fig. 3 a Shows an example disc-like particle as it dissolves. b Shows a dissolving rod-like particle with trapped air bubbles

2.1.1 Limitations

The method described in Sect. 2.1 fulfilled our goal to find a pourable recipe that creates particles capable of holding their shape as they dissolve. However, there were some limitations regarding the shelf-life of the particles and their moldability. The shelf-life, or how long a certain batch of particles can be stored, depends on their moisture content and the relative humidity the day they were made and during storage. In certain situations, the particles may become sticky during storage and start to "weep," i.e. lose their structure and have a fluctuating water content (Ergun et al. 2010). Fluctuating water content is a result of the water activity in a particle and causes structural instability, shortening the allowable storage time between manufacturing and testing.

The particles typically start with low water activity, indicating little water in the particle is available to contribute to physical or chemical processes (Ergun et al. 2010). This leads to the movement of moisture from the air to the particle surface. To visualize this, imagine finding a piece of old candy in the back of the pantry. Old candy tends to be sticky and difficult to separate from its wrapper (Hartel

et al. 2018). The old candy has increased in water content as it gains water molecules from the air around it, making it sticky.

Exchange of water molecules between air and particles is not one-directional nor is the water concentration in each medium often at equilibrium. Once the surface of the particles (or candy) starts accepting water, the total water activity of the particles will increase. As a result of the increased water activity, more water will move from the particle to the air than from the air to the particle (a net loss in water). Since the particle now has fewer water molecules than the air, it will start accepting water molecules again. The trading of water molecules from the air to the particles and back again leads to disintegration of the particles, and causes them to become soft, sticky, and lose their shape (Ergun et al. 2010). Figure 4b and d show examples of weeping particles; Fig. 4a and e show incompletely molded particles; Fig. 4c is the final recipe used.

The temperature of the recipe during cooking strongly influences the final water content of a particle as well. A batch cooked too long will have a very low water content, and, therefore, low water activity. The lower the water activity is, the more rapidly water will move from the atmosphere

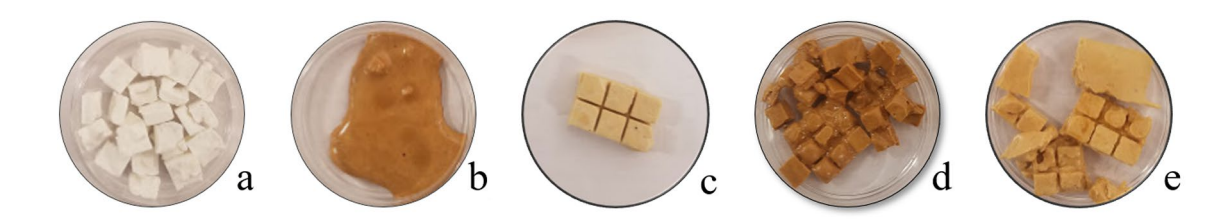


Fig. 4 Results from recipe trials. The dextrose-to-sucrose ratio is increasing from sample $\bf a$ to sample $\bf e$. $\bf a$ No dextrose, low-temp; $\bf b$ no dextrose, high-temp; $\bf c$ low dextrose-to-sucrose ratio, mid-temp; $\bf d$ low

dextrose-to-sucrose ratio, high-temp; **e** high dextrose-to-sucrose ratio, mid-temp. The side-length of each of the cubes pictured is 7.5 mm



to the particle as a result of a steeper concentration gradient. The higher gradient leads to faster decomposition of the shape and a shorter amount of time the particle can be stored before it is tested. Arriving at the ideal water content and temperature combination also influences how well the molds can be filled and leveled off. In our effort to find a procedure reliable enough for scientific study, we tested over 100 batches varying recipes and methods of mixing and molding. Small fluctuations in the initial mass of a particle were not uncommon as a result of small variations in particle manufacturing. Considering all these variations, the results are still quite clustered and repeatable (see Sect. 3). Slight departures from neutral buoyancy are visually obvious to the experimenter. Our recipe using 5.55 g of bubbles stays suspended in the tank, while the one with 5.60 g and 5.50 g go directly to the top or bottom of the tank and stay there.

2.2 Evaluation of particles

The turbulence tank described in Bellani and Variano (2014) was used to evaluate the shape dependence of the mass transfer rate. The test section of the tank is $80 \text{ cm} \times 80 \text{ cm} \times 75 \text{ cm}$ and is located in the middle of the tank between two mesh screens. The screens were used to prevent particles from going into the jet intake. Turbulence in the tank was created by two 8×8 arrays of synthetic jets, located at opposite ends of the tank, and positioned to face each other. The jets were randomly actuated in a way to maximize isotropy and minimize mean flow (Bellani and Variano 2014). The turbulence tank was filled with filtered and degassed tap water. A schematic of the tank is shown in Fig. 5.

Turbulent quantities were taken from Byron (2015) and Bellani et al. (2013) and averaged over the entire volume of the test section. The volume-averaged energy dissipation rate was $5.49 \times 10^{-5} \text{m}^2/\text{s}^3$, the volume-averaged turbulent velocity (u_{rms}) was $1.98 \times 10^{-2} \text{m/s}$, and the volume-averaged Taylor scale was $\lambda_{\tau} = 1.55 \times 10^{-2} \text{m}$. The proposed characteristic scale of interest for particle

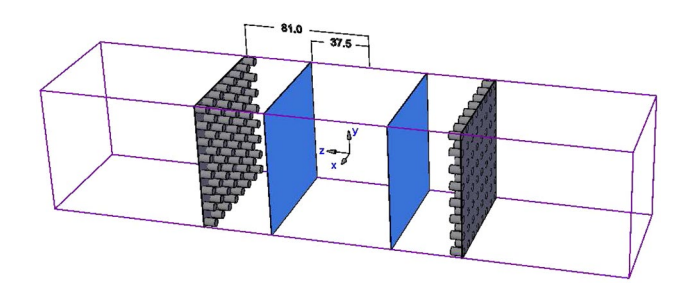
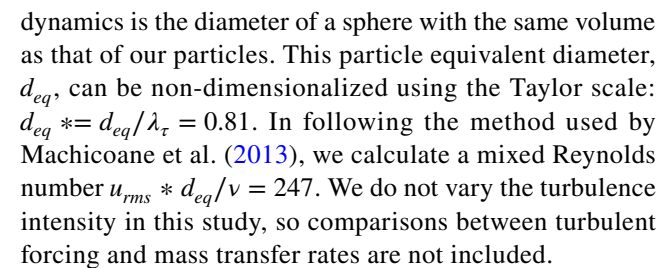


Fig. 5 Turbulence tank used to evaluate sugar-glass-sphere particles. The screens were placed in the tank to enhance flow isotropy and to keep the particles from coming into contact with the jet arrays. Units in the diagram are in centimeters. The entire length of the tank is 360 cm and the cross section is 80 cm by 80 cm



The mass transfer rate of the shapes was characterized by taking measurements of the mass of a single particle until it had completely dissolved. This was repeated oneby-one for each rod- and disc-shaped particle that was tested. Each particle was dropped into the tank while the jets were firing, and then was removed from the tank after 60-80 s using an aquarium fish net. KimwipesTM were used to prevent the particles from sticking to the scale. Once the wipe was placed on the scale, the scale was tared and the mass of the particle was measured. The mass of the particle and the amount of time it spent in the tank were recorded. After the measurements were taken, the particle was placed back in the tank so it could continue to interact with the flow. The process of removing the particle, recording the time, and recording its mass, was repeated until the particle was too small to register on the scale (less than 0.1 g). The presented data show the results of the two shapes that were tested. This experiment was repeated multiple times to check repeatability. Presented here are the results for approximately 30 disc- and 30 rod-shaped particles.

Although the rod- and disc-shaped particles became skinnier and flatter as they dissolved, they still maintained their 'rod' and 'disc' form. Evidence of this shape-similarity is shown in Fig. 3. The dissolving rod-like particles were more fragile than the disc-like particles, but they generally did not break due to handling or fluid motion unless they contained air bubbles resulting from poor manufacturing (evidence of this shown in Fig. 3b). Both types of particles held their shape until they were too small to accurately register on the weighing scale at our disposal. This success was sensitive to following the appropriate recipe and achieving the correct temperature and water content (Fig. 4c).

The neutrally buoyant particles do get stalled at boundaries, and can spend anywhere from about 2 s to 2 min there. They always leave the boundary, and the majority of time is spent in the tank and not at boundaries. Particle behavior appears to be the same at each of the boundary types (one free-slip surface, one no-slip bottom, two no-slip walls, and two porous walls). Figure 6 shows a short time-lapse (6 s at 1-s intervals) of particle motion. At the beginning of the time-lapse, the particle moved 2–3 times its length in 1 s. At the end of the time lapse, the particle was almost stationary for several seconds. The particle was not near the boundaries when these images were taken.



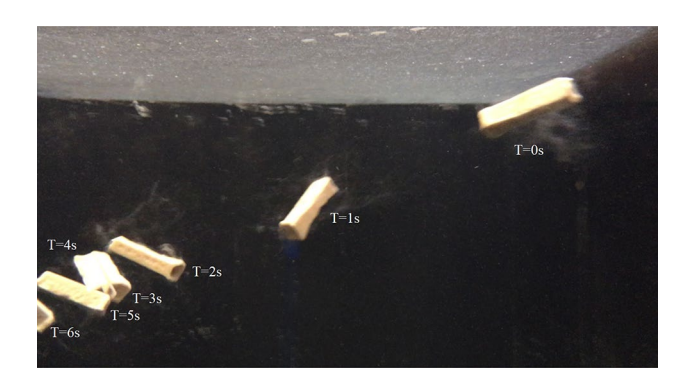


Fig. 6 Time lapse of particles suspended in turbulence tank. These images cover 6 s of particle motion. At the beginning the particle had a downward trajectory due to the momentum from being dropped in the tank. After around 2 s, the particle starts to rotate in space at approximately a constant location

3 Analysis and results

Figure 7 shows the particle mass (normalized by the particle's initial mass) as it dissolves over time. Excluding normalization, these data are unprocessed. The mass flux away from the particle is greater at early times, i.e. when the particle is larger. This is no surprise, given that surface area is larger at early times. A classic model for dissolution that is based only on geometry is the Hixson–Crowell model (Hixson and Crowell 1931). It assumes that mass flux away from the surface is a constant, and that geometry is simple enough that particle lengths decrease linearly with time. Since we are using a normalized mass, we use a model based on the percentage change of each side length.

Inspired by the Hixson–Crowell model, we assume that mass is lost normal to the surface at a constant rate k [length/time], and that all sides recede a length kt in a direction normal to the surface. Implicit in this formulation is the fact that the dissolution rate is not influenced by the accumulation of solute in the ambient fluid nor in the boundary layer close to the particle. This method has a small bias in how it handles the corners of objects, but the spread in our data suggests that it is not worth proceeding to more advanced models that integrate local fluxes around the surface.

Our model is shown in Eq. 1. Here l_0 , w_0 , and h_0 are the initial length, width, and height of the particles, respectively. V_t is the particle volume at a given time, t. We assume that density is constant, so volume and mass are linearly related.

$$V_t = (l_0 - kt)(w_0 - kt)(h_0 - kt)$$
(1)

The presented data in Fig. 7 exhibit a trend in agreement with the proposed model. In this model, we assume that the mass flux is constant for a particle freely suspended in turbulence. Results from Machicoane et al. (2013) provide

support for this assumption. Turbulence is one of several effects that are grouped into a single factor k. We cannot predict k a priori, but the new method presented herein provides a potential route to assembling a large enough dataset of dissolution rates that one could connect k to the dynamics of the unsteady boundary layer on suspended particles.

The model in Eq. 1 was fitted to the data in Fig. 7 using a non-linear, iterative least squares regression via Matlab's nlinfit routine. The single fit parameter is the dissolution rate, k. Table 1 summarizes the important calculated values. The 95% confidence interval for Fig. 7 was calculated using the Jacobian and the residuals for the fit via Matlab's nlparci ("nonlinear parameter confidence intervals") routine.

4 Discussion

In the proposed model, predicting k a priori is challenging because it combines turbulence and material properties into a single value. Nevertheless, the data from our experiments seem to fit this model relatively well. As seen in Fig. 7, the fitted curve for the rod-like data is lower and steeper than the curve for the disc-like data, indicating that the rod-like particles lose mass faster than the disc-like ones.

Table 1 Dissolution rate, k, as measured for rod- and disc-shaped particles

Particle type	Cube root dissolution rate, k_0 [cm/min]	95% Confidence interval [cm/min]	R-squared value [–]
Rod-like	0.044	[0.043 0.045]	0.970
Disc-like	0.0405	[0.040 0.041]	0.984

These values were calculated using the model presented in Eq. 1 and shown in Fig. 7

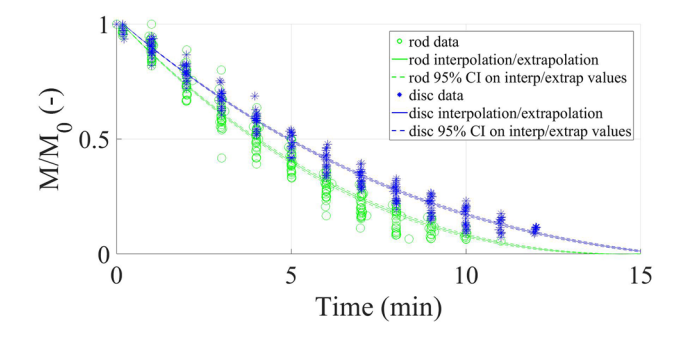


Fig. 7 The fit of the data to the proposed model. The rod-like data are shown as green circles, the disc-like data are shown as blue stars. The solid line is the fit to the data points, and the dashed line is the 95% confidence interval. Each trajectory is a single particle. Vertical variation is due to individual particle idiosyncrasy. It is seen from the slopes that the rod-like particles dissolve more rapidly than the disc-like particles



One reason rod- and disc-like particles have different dissolution rates could be due to the difference in aspect ratios which cause particles to sample the turbulence in a biased manner (Byron et al. 2015). Another reason for the different dissolution rates in volume-matched particles could be due to the difference in their specific surfaces (surface-area-to-volume ratios).

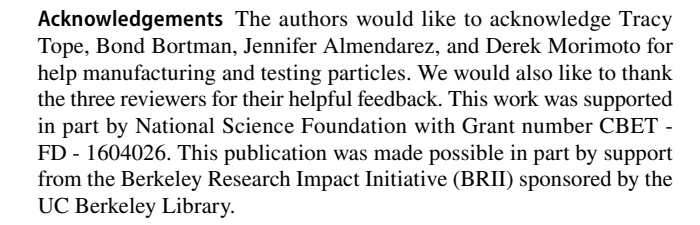
Future work using the technique presented herein will be able to cover a large enough parameter space to fit a model that parses out the different effects of shape, size, turbulence intensity, etc. For example, a model would ideally include factors for the turbulent boundary layer thickness around the particle, the dissolution rate of the particle in laminar flow, and shape effects. We would like to separate out the effect of factors such as aspect ratio, edge length, and corners and protrusions, as well as particle kinematics in turbulence, e.g. rods experiencing more 'angular slip' or sweeping out broader volumes of space as they rotate. For now, we have chosen a one-parameter model because it matches the amount of data we have.

5 Conclusion

In this paper, we present an alternative to the gypsum dissolution method for measuring mass transfer in turbulent flow. We show a successful recipe for a neutrally buoyant mixture of sugar and hollow glass spheres and a method for molding the recipe into disc- and rod-shaped particles. We found that the data followed the proposed dissolution model and that rod-shaped particles had a slightly faster dissolution rate compared to disc-shaped particles.

While we encountered challenges with molding the particles and maximizing their shelf life, we found this method to be successful. The high viscosity of the mixture and its rapid cooling time made producing sharp edges difficult. Insulating the cooking vessel helped with the overall pourability and moldability of the mixture, which increased the frequency of achieving the desired particle shape. To minimize particle degradation, accurate water content and temperature measurements were vital and ensured optimal particle composition.

Determining particle-specific dissolution rate parameters is important for understanding the shape–motion–flux relationships of dissolving objects. Additional experiments exploring the surface-area-to-volume ratio of the dissolving particles should be performed, where both the surface area and the mass are recorded at each time interval. More shapes and surface-area-to-volume ratios should also be tested along with varying the turbulence intensity to explore how the dissolution relates to d_{eq} , surface area, volume, and turbulence.



Open Access This article is licensed under a Creative Commons Attribution 4.0 International License, which permits use, sharing, adaptation, distribution and reproduction in any medium or format, as long as you give appropriate credit to the original author(s) and the source, provide a link to the Creative Commons licence, and indicate if changes were made. The images or other third party material in this article are included in the article's Creative Commons licence, unless indicated otherwise in a credit line to the material. If material is not included in the article's Creative Commons licence and your intended use is not permitted by statutory regulation or exceeds the permitted use, you will need to obtain permission directly from the copyright holder. To view a copy of this licence, visit http://creativecommons.org/licenses/by/4.0/.

References

Angradi T, Hood R (1998) An application of the plaster dissolution method for quantifying water velocity in the shallow hyporheic zone of an Appalachian stream system. Freshw Biol 39(2):301–315. https://doi.org/10.1046/j.1365-2427.1998.00280.x

Bagøien E, Kiørboe T (2005) Blind dating—mate finding in planktonic copepods. I. Tracking the pheromone trail of Centropages typicus. In: Marine ecology progress series 300, pp 105–115. https://doi. org/10.3354/meps300105

Baird ME, Atkinson MJ (1997) Measurement and prediction of mass transfer to experimental coral reef communities. Limnol Oceanogr 42(8):1685–1693. https://doi.org/10.4319/lo.1997.42.8.1685

Balachandar S, Eaton John K (2010) Turbulent dispersed multiphase flow. Ann Rev Fluid Mech 42(1):111–133. https://doi.org/10.1146/annurev.fluid.010908.165243

Gabriele B, Nole Michael A, Variano Evan A (2013) Turbulence modulation by large ellipsoidal particles: concentration effects. Acta Mech 224(10):2291–2299. https://doi.org/10.1007/s00707-013-0925-z.

Bellani G, Variano Evan A (2014) Homogeneity and isotropy in a laboratory turbulent flow. In: Experiments in Fluids 55.1. arXiv:1309.2148. https://doi.org/10.1007/s00348-013-1646-8

Bird R Byron, Stewart Warren E, Lightfoot Edwin N (2007) Transport phenomena. Rev. 2nd ed. Wiley, Amsterdam. isbn: 978-0-470-11539-8

Boon-Long S, Laguerie C, Couderc JP (1978) Mass transfer from suspended solids to a liquid in agitated vessels. Chem Eng Sci 33(7):813–819. https://doi.org/10.1016/0009-2509(78)85170-7. http://www.sciencedirect.com/science/article/pii/0009250978 851707 (visited on 06/29/2020)

Bordoloi Ankur D, Variano E (2017) Rotational kinematics of large cylindrical particles in turbulence. J Fluid Mech 815:199–222. https://doi.org/10.1017/jfm.2017.38. http://www.cambridge.org/core/journals/journal-of-fluid-mechanics/article/rotational-kinematics-of-largecylindrical-particles-in-turbulence/A9B2703BFF CF31CE133CE36BCC8D2D7E (visited on 11/18/2018)

Byron M, et al (2015) Shape-dependence of particle rotation in isotropic turbulence. In: Physics of Fluids (1994-present) 27.3, p. 035101. ISSN: 1070-6631, 1089-7666. https://doi.



- org/10.1063/1.4913501. url: http://scitation.aip.org/content/aip/journal/pof2/27/3/10.1063/1.4913501 (visited on 12/11/2016)
- Byron Margaret (2015) The rotation and translation of non-spherical particles in homogeneous isotropic turbulence. English. Ph.D. University of California, Berkeley. (Visited on 02/27/2017)
- Chang S et al (2013) Local mass transfer measurements for corals and other complex geometries using gypsum dissolution. Exp Fluids 54(7):1563. https://doi.org/10.1007/s00348-013-1563-x
- Chevillard L, Meneveau C (2013) "Orientation dynamics of small, triaxial- ellipsoidal particles in isotropic turbulence. en. In: Journal of Fluid Mechanics 737. Publisher: Cambridge University Press, pp. 571–596. https://doi.org/10.1017/jfm.2013.580. https://www. cambridge.org/core/journals/journal-offluid-mechanics/article/ orientation-dynamics-of-small-triaxialellipsoidal-particles-inisotropic-turbulence/B4EFA99CB5D0D2CA001F4197EEED18 86 (visited on 07/17/2020)
- Cisse M, Homann H, Bec J (2013) Slipping motion of large neutral-lybuoyant particles in turbulence. J Fluid Mech 735:1469–7645. https://doi.org/10.1017/jfm.2013.490. arXiv:1306.1388
- Do-Quang M, et al (2014) "Simulation of finite-size fibers in turbulent channel flows". In: Physical Review E 89.1. Publisher: American Physical Society, p. 013006. https://doi.org/10.1103/PhysRevE.89.013006. (visited on 04/13/2020)
- Ergun R, Lietha R, Hartel RW (2010) Moisture and shelf life in sugar confections. Crit Rev Food Sci Nutr 50(2):162–192. https://doi.org/10.1080/10408390802248833
- Feng P et al (2017) In situ nanoscale observations of gypsum dissolution by digital holographic microscopy. Chem Geol 460:25–36. https://doi.org/10.1016/j.chemgeo.2017.04.008. http://www.sciencedirect.com/science/article/pii/S000925411730195X
- Fornari W, et al (2016) The effect of particle density in turbulent channel flow laden with finite size particles in semi-dilute conditions. In: Physics of Fluids 28.3. Publisher: Am Inst Phys p. 033301. ISSN: 1070-6631. https://doi.org/10.1063/1.4942518. https://aip.scitation.org/doi/10.1063/1.4942518
- Grijseels H, Crommelin DJA, de Blaey CJ (1981) Hydrodynamic approach to dissolution rate. Pharmaceutisch weekblad 3(1):1005–1020. https://doi.org/10.1007/BF02193318. https://link.springer.com/article/10.1007/BF02193318 (visited on 06/08/2017
- Hartel RW, von Elbe Joachim H, Hofberger R (2018) Confectionery Science and Technology. Springer, New York. ISBN: 978-3-319-61740-4. url: https://www.springer.com/gp/book/9783319617404 (visited on 09/23/2019)
- Haugen NEL, et al (2017) The effect of turbulence on mass and heat transfer rates of small inertial particles. In: arXiv:1701.04567 [physics]. (visited on 02/23/2017)
- Hixson AW, Crowell JH (1931) Dependence of Reaction Velocity upon surface and Agitation. Ind Eng Chem 23(8):923–931. https://doi.org/10.1021/ie50260a018
- Huang Jinzi Mac, Nicholas M, Moore J, Ristroph Leif (2015) "Shape dynamics and scaling laws for a body dissolving in fluid flow". In: Journal of Fluid Mechanics 765: 1469-7645. ISSN: 0022-1120, https://doi.org/10.1017/jfm.2014.718. url: https://www. cambridge.org/core/journals/journal-of-fluid-mechanics/article/ shape-dynamics-and-scaling-lawsfor-a-body-dissolving-in-fluid -flow/ECC951C579D5850095DAFF40CD2899BA (visited on 04/25/2017)
- Kiørboe Thomas, et al (2002) "Mechanisms and Rates of Bacterial Colonization of Sinking Aggregates". en. In: Applied and Environmental Microbiology 68.8. Publisher: American Society for Microbiology Section: MICROBIAL ECOLOGY, pp. 3996-4006. ISSN: 0099-2240, 1098-5336. https://doi.org/10.1128/AEM.68.8.3996-4006.2002. url: https://aem.asm.org/content/68/8/3996 (visited on 07/13/2020)
- Levins DM, Glastonbury JR (1972) "Application of Kolmogorofff's theory to particle—liquid mass transfer in agitated vessels". en.

- In: Chemical Engineering Science 27(3): 537-543. ISSN: 0009-2509. https://doi.org/10.1016/0009-2509(72)87009-X. url: http://www.sciencedirect.com/science/article/pii/000925097287009X (visited on 07/14/2020)
- Lombard F, Koski M, Kiørboe T (2013) "Copepods use chemical trails to find sinking marine snow aggregates". en. In: Limnology and Oceanography 58.1. eprint: https://aslopubs.onlinelibrary.wiley.com/doi/pdf/ pp. 185–192. issn: 1939-5590. https://doi.org/10.4319/lo.2013.58.1.0185. url: https://aslopubs.onlinelibrary.wiley.com/doi/abs/10.4319/lo.2013.58.1.0185 (visited on 07/13/2020)
- Lucci Francesco, Ferrante Antonino, Elghobashi Said (2010) "Modulation of isotropic turbulence by particles of Taylor length-scale size". en. In: Journal of Fluid Mechanics 650. Publisher: Cambridge University Press, pp. 5-55. ISSN: 1469-7645, 0022-1120. https://doi.org/10.1017/S0022112009994022. url: http://www.cambridge.org/core/journals/journal-of-fluid-mechanics/article/modulation-of-isotropic-turbulence-by-particles-oftaylor-lengt hscale-size/250173E16E85D12B16962829E3AF08D9 (visited on 04/13/2020)
- Machicoane N, Bonaventure J, Volk R (Dec. 2013) "Melting dynamics of large ice balls in a turbulent swirling flow". In: Physics of Fluids 25.12, p. 125101. ISSN: 10706631. https://doi.org/10.1063/1.4832515. url: http://search.ebscohost.com/login.aspx?direct=true&db=a9h&AN=93390939&site=eds-live (visited on 08/26/2016)
- Nazaroff WW, Alvarez-Cohen Lisa (2001) Environmental engineering science. Wiley. ISBN: 0-471-14494-0. url: https://libproxy.berkeley.edu/login?qurl=https%3a%2f%2fsearch.ebscohost.com%2flogin.aspx%3fdirect%3dtrue%26db%3dcat04202a%26AN%3ducb.b11903619%26site%3deds-live
- Pachon-Rodriguez Edgar Alejandro, Colombani Jean (2013) "Pure dissolution kinetics of anhydrite and gypsum in inhibiting aqueous salt solutions". en. In: AIChE Journal 59.5, pp. 1622-1626. ISSN: 1547-5905. https://doi.org/10.1002/aic.13922. url: http://onlinelibrary.wiley.com/doi/10.1002/aic.13922/abstract (visited on 08/18/2016)
- Pope Stephen B (2000) Turbulent Flows. Cambridge University Press, Cambridge. ISBN 978-0-521-59886-6. https://doi.org/10.1017/ CBO9780511840531. url: https://www.cambridge.org/core/books/turbulent-flows/C58EFF59AF9B81AE6CFAC9ED16486B3A (visited on 07/17/2020)
- Porter Elka T, Sanford Lawrence P, Suttles Steven E (2000) "Gypsum dissolution is not a universal integrator of 'water motion". en. In: Limnology and Oceanography 45.1, pp. 145-58. https://doi.org/10.4319/lo.2000.45.1.0145. url: http://onlinelibrary.wiley.com/doi/10.4319/lo.2000.45.1.0145/abstract (visited on 08/18/2016)
- Pujara Nimish, Oehmke Theresa B, et al (2018) "Rotations of large inertial cubes, cuboids, cones, and cylinders in turbulence". en. In: Physical Review Fluids 3.5. ISSN: 2469-990X. https://doi.org/10.1103/PhysRevFluids.3.054605. url: https://link.aps.org/doi/10.1103/PhysRevFluids.3.054605 (visited on 06/21/2018)
- Pujara Nimish, Voth Greg A, Variano Evan A (2019) "Scale-dependent alignment, tumbling and stretching of slender rods in isotropic turbulence". en. In: Journal of Fluid Mechanics 860. Publisher: Cambridge University Press, pp. 465-486. issn: 0022-1120, 1469-7645. https://doi.org/10.1017/jfm.2018.866. url: https://www.cambridge.org/core/journals/journalof-fluid-mechanics/article/scaledependent-alignment-tumbling-and-stretchingof-slender-rods-in-isotropic-turbulence/0F3D07A60E48E32874F43F0AA CD4E12B (visited on 07/17/2020)
- Sano Y, Yamaguchi N, Adachi T (1974) Mass transfer coefficients for suspended particles in agitated vessels and bubble columns. J Chem Eng Jpn 7(4):255–261. https://doi.org/10.1252/jcej.7.255



Sasson DA, Jacquez AA, Ryan JF (2018) The ctenophore Mnemiopsis leidyi regulates egg production via conspecific communication. BMC Ecol 18(1):12. https://doi.org/10.1186/s12898-018-0169-9

- Shima P, Voth Greg A (2014) Inertial Range Scaling in Rotations of Long Rods in Turbulence. Physical Review Letters 112(2):024501. https://doi.org/10.1103/PhysRevLett.112.024501
 1. url: https://link.aps.org/doi/10.1103/PhysRevLett.112.024501
 (visited on 11/16/2017)
- Stocker R, et al (2008) Rapid chemotactic response enables marine bacteria to exploit ephemeral microscale nutrient patches". en. In: Proceedings of the National Academy of Sciences 105.11. Publisher: National Academy of Sciences Section: Biological Sciences, pp. 4209-4214. ISSN: 0027-8424, 1091-6490. https://doi.org/10.1073/pnas.0709765105. url: https://www.pnas.org/content/105/11/4209 (visited on 07/13/2020)
- Thompson T Lewis, Glenn Edward P (1994) "Plaster Standards to Measure Water Motion". Limnology and Oceanography 39(7):1768-1779. ISSN: 0024-3590. url: http://www.jstor.org/stable/2838211 (visited on 08/26/2016)
- Uhlmann M (2008) "Interface-resolved direct numerical simulation of vertical particulate channel flow in the turbulent regime". In:

- Physics of Fluids 20.5. Publisher: American Institute of Physics, p. 053305. ISSN: 1070-6631. https://doi.org/10.1063/1.2912459. url: https://doi.org/10.1063/1.2912459 (visited on 04/13/2020)
- Voth Greg A (2015) "Disks aligned in a turbulent channel". en. In: Journal of Fluid Mechanics 772. Publisher: Cambridge University Press, pp. 1-4. ISSN: 0022-1120, 1469-7645. https://doi.org/10.1017/jfm.2015.144. url: http://www.cambridge.org/core/journals/journal-offluid-mechanics/article/disks-aligned-in-aturbulent-channel/5C80382BEEE9661E02A03FF5B5BF7528 (visited on 04/13/2020)
- Voth GA, Soldati A (2017) Anisotropic particles in turbulence. Annu Rev Fluid Mech 49(1):249–276. https://doi.org/10.1146/annurev-fluid-010816-060135

Publisher's Note Springer Nature remains neutral with regard to jurisdictional claims in published maps and institutional affiliations.

